HHS Public Access

Author manuscript

Mol Cell. Author manuscript; available in PMC 2020 July 25.

Published in final edited form as:

Mol Cell. 2019 July 25; 75(2): 382–393.e5. doi:10.1016/j.molcel.2019.05.020.

Oxygen-dependent interaction between FBXL5 and CIA targeting complex regulates iron homeostasis

Adarsh K. Mayank[1,#], **Vijaya Pandey**[1,#], **Ajay A. Vashisht**[1,2], **William D. Barshop**[1], **Shima Rayatpisheh**[1], **Tanu Sharma**[1,2], **Tisha Haque**[1], **David N. Powers**[1,3], **James A. Wohlschlegel**[1,*]

[1]Department of Biological Chemistry, David Geffen School of Medicine at UCLA, Los Angeles, CA, USA.

[2]Current Address: Genomics Institute of the Novartis Research Foundation, La Jolla, CA, USA.

[3]Current Address: U.S. Food and Drug Administration, CDER, Silver Spring, MD, USA.

Summary

The iron sensing protein FBXL5 is the substrate adaptor for a SKP1-CUL1-RBX1 E3 ubiquitin ligase complex that regulates the degradation of iron regulatory proteins (IRPs). Here we describe a mechanism of FBXL5 regulation involving its interaction with the cytosolic Fe-S cluster assembly (CIA) targeting complex comprised of MMS19, FAM96B, and CIAO1. We demonstrate that the CIA targeting complex promotes the ability of FBXL5 to degrade IRPs. In addition, the FBXL5-CIA targeting complex interaction is regulated by oxygen tension displaying a robust association in 21% O_2 that is severely diminished in 1% O_2 and contributes to O_2-dependent regulation of IRP degradation. Together, these data identify a novel oxygen-dependent signaling axis that links IRP-dependent iron homeostasis with the Fe-S cluster assembly machinery.

Graphical Abstract

[*]Corresponding Author and Lead Contact: jwohl@ucla.edu.
[#]These authors contributed equally to the work.

Author Contributions

AKM, VP, AAV, and JAW designed experiments and analyzed the data. AKM, VP, and AAV performed experiments with assistance from SR, TS, TH, TC, and DNP. Mass spectrometry experiments were performed by WDB. AKM, VP, and JAW wrote the manuscript.

Declaration of Interest

None

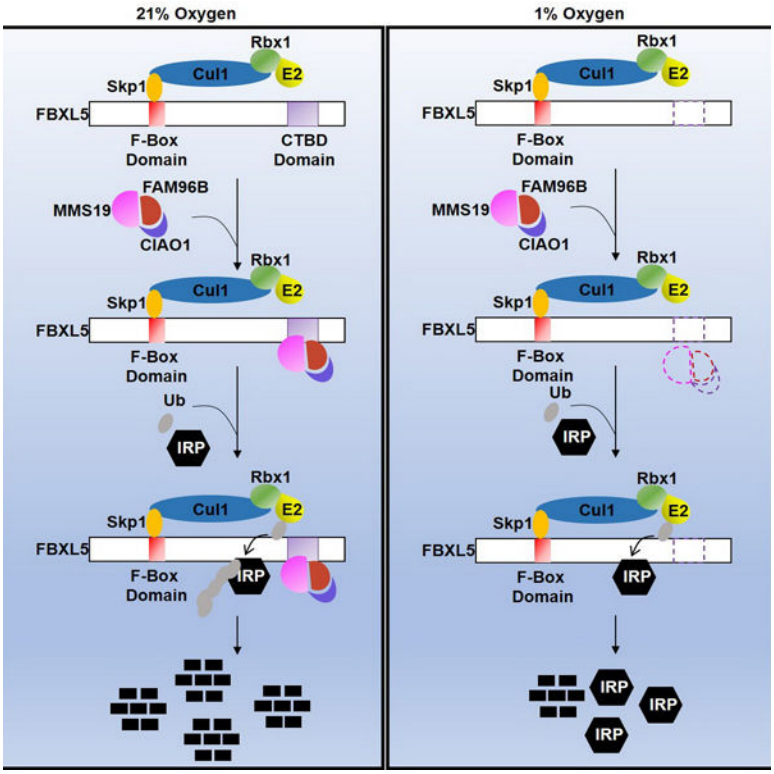

eTOC Blurb

Mayank et al. describes a mechanism of crosstalk between the iron homeostasis and Fe-S cluster biogenesis pathways that is mediated by an interaction between the iron sensor FBXL5 and the CIA targeting complex which assembles cofactors on cytosolic proteins. This mechanism is required for the proper regulation of these pathways.

Introduction

Iron is an essential element involved in basic biological processes including enzymatic catalysis, mitochondrial respiration, DNA replication and repair. Given its significance in fundamental biochemical events and the deleterious effects associated with its excess or deficiency, it is unsurprising that iron levels are delicately regulated in biological systems (Torti and Torti, 2013). Cellular iron homeostasis is maintained by finely tuned levels of iron-regulatory proteins, IRP1 and IRP2, that regulate the post-transcriptional expression of key genes involved in iron import (TFRC), export (FPN1) and storage (FTH1 and FTL) (Muckenthaler et al., 2016). IRPs bind to *cis*-regulatory iron-responsive elements (IREs) located in the untranslated regions of target mRNAs regulating their translation initiation and/or stability. Although IRP binding to IREs is iron-dependent, IRPs are unable to directly perceive changes in cellular iron levels. In iron-replete (and high O_2 tension) conditions, IRP2 is earmarked for proteasomal degradation by a ubiquitin-ligase protein complex comprised of the substrate adaptor FBXL5 and accessory factors SKP1 and CUL1 (Vashisht et al., 2009; Salahudeen et al., 2009). FBXL5 senses iron via its N-terminal hemerythrin-like domain (Hr) which binds iron and stabilizes the protein. However, during iron scarcity, the

Hr domain becomes unfolded triggering its own proteasomal degradation and the accumulation of IRP2 levels.

Fe-S clusters are redox cofactors required by proteins involved in functions ranging from transcriptional regulation and DNA metabolism to iron homeostasis (Rouault and Maio, 2017). In mammalian cells, Fe-S cluster biogenesis is mediated by a well-orchestrated, highly compartmentalized pathway consisting of both cytoplasmic and mitochondrial protein complexes dedicated to their assembly (Sharma et al., 2010). In the cytoplasmic branch of this pathway, Fe-S clusters are delivered to apo-proteins via the cytosolic iron sulfur cluster assembly (CIA) targeting complex, comprised of MMS19, FAM96B and CIAO1. This complex facilitates the transfer of Fe-S clusters from upstream CIA components to apo-proteins involved in nucleotide and DNA metabolism such as xeroderma pigmentosum protein D (XPD), regulator of telomere length protein 1 (RTEL1) and Fanconi anemia protein J (FANCJ) (Stehling et al., 2012; Gari et al., 2012). Recent developments also point to the potential involvement of CIA targeting machinery in regulating iron homeostasis. Specifically, IRP2 levels have been shown to accumulate upon depletion of either MMS19 or FAM96B (Stehling et al., 2013).

In the present study, we have further probed the link between the CIA targeting pathway and regulation of iron homeostasis. We examined the interactome of FBXL5 and identified interactions between FBXL5 and three components of late acting CIA machinery: MMS19, FAM96B, and CIAO1. These CIA components are not substrates of FBXL5-dependent ubiquitination but instead promote FBXL5-dependent IRP degradation. Furthermore, we identify a domain called **C**IA-**t**argeting-complex **b**inding **d**omain (CTBD) within FBXL5 that is essential for binding to the MMS19-FAM96B-CIAO1 complex. Disruption of the interaction between FBXL5 and the CIA targeting complex, either due to deletion of the CTBD or low O_2 tension in cells, severely diminishes the ability of FBXL5 to drive IRP poly-ubiquitination and degradation.

Results

FBXL5, an E3 ubiquitin ligase substrate adaptor protein, interacts with CIA targeting complex.

Affinity purification followed by mass spectrometry (AP-MS) was used to identify binding partners of 3HA-3Flag-tagged human FBXL5 stably expressed in Flp-In-293 cells. This analysis identified all three components of the CIA targeting complex (MMS19, CIAO1, FAM96B) as significantly enriched in the FBXL5 immunoprecipitates (Fig.1A and Table S1). To validate this observation, we performed co-immunoprecipitation analyses in cells stably expressing either HA-Flag-tagged wild-type FBXL5 or FBXL5-ΔFbox, a dominant negative mutant of FBXL5 that is defective in Skp1 binding rendering it unable to incorporate into an active SCF^{FBXL5} E3 ubiquitin ligase complex. Endogenous MMS19, FAM96B and CIAO1 co-purified with both wild-type FBXL5 and the ΔFbox mutant (Fig. 1B). Together, these results identify a novel interaction between FBXL5 and the CIA targeting complex with potential implications for the interplay between iron homeostasis and Fe-S cluster assembly pathways.

CIA Targeting Complex is not a substrate of FBXL5-E3 ubiquitin ligase complex.

To examine the functional relevance of the FBXL5 – CIA targeting complex interaction, we tested the hypothesis that the CIA targeting complex was targeted by FBXL5 for ubiquitin-dependent degradation in a relationship analogous to the FBXL5-IRP2 interaction. First, we compared the interaction of the CIA targeting complex with either wildtype FBXL5 or FBXL5-ΔFbox. In contrast to IRP2 which is stabilized by and preferentially co-precipitates with FBXL5-ΔFbox, the CIA targeting complex interacts equally well with both the wild-type and mutant forms of FBXL5 suggesting that the interaction may differ from the hypothesized E3-substrate relationship (Fig. 1B). Consistent with this idea, FBXL5 overexpression stimulates the ubiquitin-dependent degradation of IRP2 without affecting the levels of MMS19, FAM96B or CIAO1 (Fig. 1B). We also tested the effects of changes in cellular iron levels on the endogenous protein levels of CIA targeting complex components. In high iron conditions, FBXL5 accumulates leading to IRP2 downregulation while in iron deficient conditions, FBXL5 is itself degraded resulting in IRP2 stabilization. If a CIA targeting complex component was a substrate of FBXL5, we would likewise expect it to be degraded in high iron and stabilized in low iron. In Fig. 1C, changes in iron levels failed to exert any significant effect on levels of MMS19 and FAM96B despite major changes in FBXL5 levels. Furthermore, depletion of endogenous FBXL5 either by siRNA or a CRISPRi/dCas9 transcriptional repression strategy also resulted in no significant changes in MMS19 or FAM96B levels (Fig. 1D and 1E). Together, these observations establish that CIA targeting complex levels are not affected by perturbation of FBXL5 levels and is consistent with the model that the CIA targeting complex is not a substrate of SCF^{FBXL5}-dependent ubiquitination under the conditions examined. However, it is important to note that these results do not rule out a role for FBXL5 in regulating Fe-S cluster biogenesis either indirectly or via its interaction with the CIA targeting complex through an undiscovered non-proteolytic mechanism. Similarly, we cannot exclude the possibility that FBXL5 can regulate the degradation of the CIA targeting complex under a distinct set of conditions not examined here.

CIA targeting complex potentiates IRP2 poly-ubiquitination and degradation.

Having established that the relationship between FBXL5 and the MMS19-FAM96B-CIAO1 complex may not be that of E3 ubiquitin ligase and substrate, we tested the possibility that the CIA targeting complex was instead influencing the FBXL5-IRP2 axis. To this end, we examined the levels of the FBXL5 substrate IRP2 in cells stably over-expressing either MMS19 or FAM96B. Compared to control cells, IRP2 levels were markedly diminished upon MMS19 overexpression (Fig. 2A). The effect of FAM96B overexpression on IRP2 levels is slightly attenuated in comparison to MMS19 overexpression which is likely due to previously reported protein homeostatic mechanisms that downregulate endogenous FAM96B upon long-term overexpression of exogeneous FAM96B in order to maintain FAM96B protein levels. In contrast to overexpression, siRNA or shRNA-mediated knockdown of MMS19 or FAM96B led to significant up-regulation of IRP2, which was concomitant with diminution of FBXL5 levels (Fig. 2B and 2C). The pattern for IRP1 expression appeared to behave similarly although the effects were much weaker than was seen with IRP2 raising questions regarding its potential significance (Fig. 2B and 2C). The positive influence of FAM96A overexpression on IRP2 levels as shown in Fig. 2A has been

reported previously and has been suggested to exert a stabilizing effect on IRP2 protein levels (Stehling et al., 2013). Further, the reduction in FAM96B levels observed upon MMS19 depletion as shown in Fig. 2B has also been described earlier (Odermatt and Gari, 2017). Consistent with these observations, we also observed that IRP2 stability drops sharply in cells overexpressing FAM96B when exposed to high iron levels and that this decrease in stability is FBXL5-dependent (Fig. S1). Based on the reciprocity of IRP2 and FBXL5 levels in response to changes in CIA targeting complex abundance, we asked if the CIA targeting complex influences the ability of FBXL5 to stimulate IRP2 poly-ubiquitination and degradation. Using cell-based ubiquitination assays, we analyzed the ubiquitination of Flag-IRP2 upon overexpression of MMS19 and FAM96B. HA-ubiquitin, Flag-IRP2 and CFP-MMS19 or CFP-FAM96B were co-expressed in HEK293 cells followed by purification of the ubiquitin conjugates under denaturing conditions using anti-HA antibodies. MMS19, FAM96B and CIAO1 overexpression led to increased FLAG-IRP2 ubiquitination (Fig. 2D). Further, this observed ubiquitination was dependent upon the E3 ubiquitin ligase activity of SCF^{FBXL5} complex since co-expression of FAM96B with the FBXL5-ΔFbox dominant negative mutant failed to increase the poly-ubiquitination of Flag-IRP2 relative to wild-type FBXL5 (Fig. 2E). Together, these results indicate that overexpression of CIA targeting complex modulates poly-ubiquitination of IRP2 by FBXL5. Since CIAO1 forms mutually exclusive complexes with MMS19, FAM96B and with FAM96A (this study and Stehling et al, 2013), with opposing ramifications for IRP2 stability, the effect of CIAO1 manipulation on iron homeostasis was not explored further here.

To probe the mechanism underlying the regulation of FBXL5 by the CIA targeting complex, we tested whether the CIA targeting complex influenced the FBXL5-IRP2 interaction by measuring the ability of IRP2 to coimmunoprecipitate with FBXL5-ΔFbox in cells depleted of either MMS19 or FAM96B. The dominant negative FBXL5-ΔFbox mutant was used instead of wild-type FBXL5 was used to ensure that IRP2 was stabilized and that we could monitor the interaction under conditions in which IRP2 was not being actively degraded. Interestingly, depletion of either MMS19 or FAM96B weakened the interaction between FBXL5-ΔFbox and IRP2 (Fig. 2F and 2G). This was not an indirect effect of down-regulation of FBXL5ΔFbox caused by depletion of CIA targeting complex proteins (Fig. 2G). These results indicate that one of the mechanisms by which the CIA targeting complex can regulate the FBXL5-IRP2 axis is by enhancing the physical interaction between FBXL5 and IRP2 leading to more efficient substrate recruitment.

FBXL5 interacts with MMS19 and FAM96B via domain comprised of 470–592 aa at its C-terminus.

Given the strong interaction between FBXL5 and the CIA targeting complex, we next sought to identify the binding interface of the interaction and the functional consequences of deletion of the interface. We generated mutants of FBXL5 that lacked various domains and examined their ability to interact with the CIA targeting complex by co-immunoprecipitation. Of the mutants tested (data not shown), one mutant lacking a region spanning amino acids 470–592 of the FBXL5 protein was impaired in its ability to interact with the CIA targeting complex (Fig. 3A). As shown in Fig. 3B and Fig. S2A, both

endogenous and GST-FAM96B interacted robustly with wildtype FBXL5 and a C-terminal fragment of FBXL5 lacking the N-terminal hemerythin domain (C500), but failed to bind to the Δ470–592 mutant. Similarly, endogenous MMS19 interacted strongly with wildtype FBXL5 and FBXL5-C500 but was unable to associate with the FBXL5-Δ470–592 and FBXL5-C500-Δ470–592 mutants (Fig. 3C). To determine whether this region of FBXL5 is sufficient for the FBXL5-CIA targeting complex interaction, we co-expressed either CFP-MMS19 or CFP-FAM96B with the Myc-FBXL5–470-592 fragment. Fig. 3D shows that the FBXL5 fragment spanning amino acids 470–592 is sufficient to mediate the MMS19 and FAM96B interactions. We have termed this 470–592 amino acid region of FBXL5 as the **C**IA-**T**argeting complex-**B**inding-**D**omain (CTBD).

Cysteine residues on proteins participate in multitude of functions, including redox reactions, allosteric regulation and metal binding. We observed multiple cysteine residues in the CTBD of FBXL5 that were conserved across human, mouse, bovine and orangutan species (Fig. S2B). To examine the potential significance of these residues in the interaction between FBXL5 and CIA targeting complex, we constructed mutants of CTBD in which these cysteines were substituted with either alanines or serines and tested their ability to interact with the CIA targeting complex. As shown in Fig. 3E, wild-type CTBD interacts robustly with MMS19, FAM96B and CIAO1, while the CTBD cysteine mutants fail to do so. These results indicate that FBXL5 binds to CIA targeting complex via the CTBD in a manner that depends on conserved cysteine residues within the CTBD for the interaction.

We also defined the binding interface between FBXL5 and the CIA targeting complex to help elucidate the organization of the two complexes. We generated FAM96B mutants lacking various regions and tested them for their ability to interact with FBXL5. As shown in Fig. S2C, full length FBXL5 interacts with a FAM96B mutant expressing amino acids 1–110 but not amino acids 1–103 suggesting the interaction is mediated by the seven amino acids spanning residues 104–110 of FAM96B. Substitution of these residues with alanine leads to loss of binding between the mutant and FBXL5. Although the FAM96B 1–110 aa fragment binds FBXL5, it fails to interact with MMS19 and CIAO1 suggesting that FBXL5 interacts with FAM96B independently of MMS19 and CIAO1. In agreement with our observation, an earlier report has shown that MMS19 interacts with FAM96B at its extreme C-terminus (Odermatt and Gari, 2017), a region that does not overlap with the FBXL5 binding region.

We also characterized the interaction of FBXL5 with other proteins of CIA targeting complex, we designed mutants of MMS19 lacking either the N-terminal region termed MMS19-ΔN (328–1030 amino acids) or the C-terminal region termed as MMS19-ΔC (1–705 amino acids). As shown in Fig. S2D, FBXL5 interacts with full length MMS19 (MMS19-WT) and MMS19-ΔN but not with the MMS19-ΔC mutant. Other components of the CIA targeting complex (e.g. FAM96B and CIAO1) display binding patterns identical to FBXL5 in that they interact with full length MMS19 and MMS19-ΔN but lose their interaction with the MMS19-ΔC mutant (Fig. S2E). Based on these results which suggest that the same region of MMS19 mediates both the FBXL5 and FAM96B interactions, we hypothesize that FBXL5 binds to MMS19 indirectly via its association with FAM96B. Together with the FBXL5-FAM96B interaction studies in Fig. S2C, these observations are

consistent with the idea that FBXL5 interacts directly with FAM96B which then mediates its association with the rest of the CIA targeting complex.

FBXL5-ΔCTBD is not as potent as wild-type FBXL5 in driving IRP2 Degradation

We observed that steady state IRP1 and IRP2 levels accumulate to higher levels in cells overexpressing FBXL5-ΔCTBD relative to wild-type FBXL5 despite FBXL5-ΔCTBD being expressed at significantly higher levels (Fig. 4A and 4B). To examine the effects of FBXL5-ΔCTBD expression more closely without the potentially confounding variable of endogenous FBXL5 expression, we generated dCas9/CRISPRi cell lines that enable us to transcriptionally repress the endogeneous *FBXL5* gene and then express either HA-FLAG-FBXL5 or HA-FLAG-ΔCTBD in the FBXL5-depleted background. As expected, cells depleted of endogenous FBXL5 accumulated high levels of IRP2 under iron-replete conditions which typically trigger IRP2 degradation; a phenotype which was readily rescued by overexpression of full-length FBXL5 (Fig. 4C). However, the ΔCTBD mutant failed to effectively down-regulate IRP2 levels in this same experimental system (Fig. 4C).

Based on our observation in Fig. 2F that MMS19 and FAM96B are required for optimal binding of IRP2 by FBXL5, we also examined whether deletion of CTBD impaired the interaction between the mutant and IRPs and thus contributed to the compromised ability of FBXL5-ΔCTBD to down-regulate IRPs (Vashisht et al., 2009; Salahudeen et al., 2009). As shown in Fig. 4D and 4E, FBXL5-ΔCTBD interacted more weakly with both IRP1 and IRP2 compared to wild-type FBXL5 indicating that removal of the CTBD compromises the ability of FBXL5 to bind substrates. The reduced capacity of FBXL5-ΔCTBD to interact with IRP2 relative to wildtype FBXL5 was also observed in in vitro binding assays using partially purified components (Fig. S3A and S3B). Together with Fig. 2F, these observations suggest that the interaction of FBXL5 with components of CIA targeting machinery via its CTBD domain strengthens the binding of FBXL5 to IRPs and contributes to their degradation.

To understand the importance of CTBD region in greater detail, we measured the rate of IRP2 degradation in doxycycline-inducible stable cell lines after induction of either full-length FBXL5 or FBXL5-ΔCTBD mutant. As shown in Fig. 4F, while protein levels of FBXL5 and FBXL5-ΔCTBD seemed comparable, there was significantly higher accumulation of IRP1 and IRP2 at early time points upon FBXL5-ΔCTBD overexpression relative to full-length FBXL5. These results suggest that the FBXL5-ΔCTBD mutant is impaired in its ability to catalyze ubiquitin-dependent IRP2 degradation. To test this hypothesis, we performed cell-based ubiquitination assays to assess IRP2 ubiquitination upon overexpression of wildtype FBXL5 or FBXL5-ΔCTBD mutant. HA-ubiquitin, Flag-IRP2 and Myc-FBXL5 or Myc-FBXL5-ΔCTBD were co-expressed in HEK293 cells and HA-ubiquitin conjugates were immunopurified. While wildtype FBXL5 triggered robust poly-ubiquitination of Flag- IRP2, FBXL5-ΔCTBD was not as potent in this function (Fig. 4G and 4H). The quantitation of IRP2 polyubiquitination after normalization to the expression level of FBXL5-wildtype and FBXL5-ΔCTBD reveals that the extent of substrate polyubiquitination by wild-type FBXL5 far exceeds that of the mutant despite higher expression levels of the FBXL5-ΔCTBD mutant (Fig. 4H). In agreement with these observations, IRP1 polyubiquitination was also attenuated by overexpression of the FBXL5-

ΔCTBD mutant compared to its wild-type counterpart (Fig. S3C and S3D). Together, these data indicate that the interaction between the CIA targeting complex and FBXL5 via the CTBD domain is important for regulating FBXL5's ubiquitin ligase activity and thus control IRP levels.

Physiological relevance of the interaction between FBXL5 and CIA targeting complex.

Hemerythrin domains bind molecular oxygen via two iron atoms coordinated by carboxylate groups and a μ-oxo-bridge (Ruiz and Bruick, 2014). Previous reports have shown that FBXL5 possesses a hemerythrin domain that confers sensitivity to both iron and molecular oxygen (Vashisht et al., 2009; Salahudeen et al., 2009; Ruiz and Bruick, 2014). In low O_2 conditions, the Hr domain adopts a conformation that promotes its own degradation. However, whether other O_2-mediated regulatory mechanisms for FBXL5 exist beyond the Hr domain remains unclear. Further, while it is well documented that Fe-S clusters can be oxygen labile and prone to oxidation under certain conditions (Fuss et al., 2016), the regulation of the CIA targeting machinery in response to changes in oxygen tension has not been thoroughly examined. Hence, we sought to probe the effect of changes in O_2 tension on the interaction between FBXL5 and the CIA targeting complex. As shown in Fig. 5A, the interaction between FBXL5 and MMS19 was dramatically reduced in cells incubated in 1% O_2 as compared to 21% O_2 (Fig. 5A). Importantly, while control cells displayed increased levels of IRP1 and IRP2 upon exposure to low O_2 as compared to 21% O_2, FBXL5 overexpression in hypoxic cells mitigated IRP accumulation (Fig.5A). Conversely, IRPs continued to accumulate in cells overexpressing FBXL5-ΔCTBD under hypoxic conditions. While MMS19 levels were not affected by changes in O_2 tension, FBXL5 wild-type and FBXL5-ΔCTBD were both down-regulated in low O_2 conditions (Fig. 5A). To test if the diminished interaction between MMS19 and FBXL5 in hypoxia was a consequence of reduced FBXL5 levels, co-immunoprecipitation assays were conducted in cells exposed to low O_2 levels but simultaneously treated with ferric ammonium citrate to stabilize FBXL5 protein levels. Although the addition of iron stabilized FBXL5 and FBXL5-ΔCTBD relative to untreated cells, the increased FBXL5 levels failed to rescue the interaction between CIA targeting complex components and FBXL5 in hypoxic cells (Fig. S4). These results indicate that the reduced interaction between FBXL5 and the CIA targeting complex in hypoxic cells is not a mere consequence of decrease in levels of FBXL5.

Next, we examined whether the IRPs that accumulated in hypoxic cells were functional and capable of regulating IRE-containing mRNAs. We addressed this question by measuring the IRE-binding activity of IRP1 and IRP2 in hypoxic cells using IRE-motif containing biotin-labeled oligonucleotides. As shown in Fig. 5B, the IRE-binding activity of IRP2 was higher in FBXL5-ΔCTBD expressing cells exposed to hypoxic conditions relative to FBXL5-WT expressing cells. Flp-In-293 cells treated with iron chelator desferal (DFO) were used as a positive control for the IRE-binding activity by IRPs. Together, we conclude that IRP2 accumulates to higher levels in FBXL5-ΔCTBD-expressing cells relative to wildtype FBXL5-expressing cells during hypoxia and that these accumulated IRPs are functional with respect to RNA binding.

To further confirm the functionality of the IRPs that accumulate in FBXL5-ΔCTBD-expressing cells, we measured steady state mRNA expression of IRE-regulated genes in cells overexpressing wild-type and ΔCTBD mutant of FBXL5. As shown in Fig. S5, overexpression of FBXL5-ΔCTBD, led to up-regulation of the relative mRNA levels of *DMT1* and *TfR1* as compared to wildtype FBXL5 overexpression even when cells were subjected to high oxygen tension. We attribute this observation to the accumulation of IRP2 that results from attenuated ability of FBXL5-ΔCTBD to support IRP2 degradation. These oresults provide further support that the pool of IRP½ regulated by FBXL5 in this pathway is functional with respect to the regulation of gene expression.

To determine the mechanism underlying the increased IRP stability in hypoxic cells, we exposed uninduced cells stably expressing inducible FBXL5 or FBXL5-ΔCTBD to 1% O_2 for 16 hours. Post-hypoxia treatment, cells were shifted to 21% O_2, treated with doxycycline to induce expression of FBXL5 or FBXL5-ΔCTBD, and harvested at regular time intervals. As shown in Fig. 5C, IRP2 levels decreased sharply upon exposure to 21% O_2 in cells expressing wild-type FBXL5. However, IRP2 levels were maintained at high levels for at least 24 hours after transfer to 21% O_2 conditions in cells overexpressing FBXL5-ΔCTBD. These results indicate that the stabilization of IRP2 that occurs in response to hypoxic conditions may be attributed, at least in part, to the observed loss of interaction between FBXL5 and the CIA targeting complex that occurs in that context.

Since the hypoxia inducible factor HIF1α is the main transcription factor induced in response to hypoxia (Majmundar et al., 2010), we examined if the disruption of the CIA targeting complex - FBXL5 interaction observed as a function of changes in O_2 tension was dependent upon HIF1α. We tested this possibility by examining how the interaction between FBXL5 and the CIA targeting complex is affected by cobalt chloride, a well-established chemical inducer of hypoxia (Wu and Yotnda, 2011). While exposing cells to 100μM $CoCl_2$ led to accumulation of HIF1α, it failed to disrupt the interaction of FBXL5 with either MMS19 or FAM96B (Fig. 5D). Similarly, the interaction between FBXL5 and MMS19 was unaffected by treatment with DMOG, a chemical inhibitor of prolyl-hydroxylases (PHD) that leads to the stabilization of HIF1α independently of oxygen tension (Fig. S6). Together, these observations suggest that the interaction is not regulated by HIF1α signaling but some other mechanism of hypoxia-induced regulation.

Discussion

Understanding how the iron homeostatic machinery responds to environmental cues to orchestrate a complex regulatory program remains a key question in the field. We describe a novel interaction between FBXL5, the ubiquitin ligase that controls IRP activity, and the CIA targeting complex, a protein complex that required to facilitate Fe-S cluster transfer to apoprotein substrates during extramitochondrial Fe-S protein biogenesis. Surprisingly, the CIA targeting complex does not appear to be a substrate of FBXL5-dependent degradation but instead acts as an allosteric effector that influences both FBXL5 stability and its activity toward IRPs. We also demonstrate that this interaction is impaired in hypoxia. These findings support a model shown in Fig. 6. In 21% O_2, the CIA targeting complex associates with FBXL5 and promotes IRP2 ubiquitination. Conversely, the FBXL5 - CIA targeting

complex interaction is abolished in 1% O_2 leading to diminished IRP2 ubiquitination and its resulting stabilization.

FBXL5 plays a major role in sensing intracellular iron levels and regulating the levels of key iron homeostatic proteins in order to ensure iron availability for cellular processes. Given that Fe-S cluster biogenesis is a major route for iron usage, the coordinate regulation of the FBXL5-IRP axis with the CIA machinery to provide FBXL5 with upstream signals detailing the activity and/or integrity of the Fe-S cluster pathways would provide a novel avenue for crosstalk between these two processes. Importantly, a role of the Fe-S cluster assembly machinery in regulating iron homeostasis is evolutionarily conserved despite major differences in the overall architecture of the iron homeostatic pathways. For example, iron homeostasis in budding yeast is controlled by the Aft1/Aft2 transcription factors which initiate a gene expression program in response to iron deficiency. During iron replete conditions, however, an Fe-S cluster-bound Grx3-Grx4 complex inactivates Aft1/Aft2-dependent transcription (Outten and Albetel, 2013). Thus, in both the human and yeast systems, Fe-S cluster assembly pathways directly influence the central regulatory axis for iron homeostasis.

A recent report has highlighted the existence of a cytosolic pathway for Fe-S cluster biogenesis that is dependent on the cochaperone HSC20 (Kim et al, 2018). In this pathway, HSC20 participates in a multiprotein complex comprised of CIA targeting complex components and is required for the delivery of Fe-S clusters to cytosolic and nuclear recipient proteins. It will be important to investigate how the FBXL5-CIA targeting complex regulatory axis discovered here may influence HSC20-dependent Fe-S cluster assembly or vice versa in order to better understand the biochemical mechanisms underlying the intersection of IRP-regulated iron homeostasis and the cytosolic Fe-S cluster biogenesis pathway.

Our findings suggest potential mechanisms by which the interaction of the CIA targeting complex with FBXL5 could influence the ubiquitin-dependent degradation of IRPs. We observe that the depletion of CIA targeting machinery components impairs the interaction of FBXL5 with IRPs (Fig. 2F). Additionally, data shown in Figs. 4D, 4E and S6 demonstrate that loss of CTBD domain, via which FBXL5 interacts with CIA targeting complex, compromises the ability of FBXL5 to interact with its substrates. Together these findings support a mechanism in which the CIA targeting complex enhances the ability of FBXL5 to bind to IRPs.

The ability of the CIA targeting complex to regulate the FBXL5-IRP2 axis is not necessarily limited to promoting substrate binding. We further envision at least three possibilities that could explain the interplay between FBXL5 and CIA targeting complex. First, FBXL5 may be a substrate that acquires a Fe-S cluster from the CIA targeting complex which is required for FBXL5 function and/or binding to IRP2. It is known that cysteine residues form ligands for Fe-S clusters in both the Fe-S cluster assembly machinery and client proteins (Rouault and Maio, 2017). Intriguingly, we note that the CTBD of FBXL5 appears enriched in cysteine residues that are conserved across mammals (Fig. S3) and that these cysteine residues are required for the FBXL5 - CIA targeting complex interaction (Fig. 3E). We

showed previously that apo-proteins interact with CIA targeting complex in order to acquire Fe-S clusters crucial for their function (Stehling et al., 2012). Many of these recipient proteins are destabilized and lose activity upon depletion of components of CIA targeting machinery. In a similar fashion, the CIA targeting complex has a stabilizing effect on FBXL5 protein levels (Fig. 2A–C) and stimulates IRP2 poly-ubiquitination (Fig. 2D). Additionally, the ΔCTBD mutant of FBXL5, which is incapable of binding CIA targeting complex, is impaired in its ability to promote IRP degradation (Fig. 4G and 4H; Fig. S7A and S7B). Together, these observations warrant investigating FBXL5 as a potential client of CIA targeting complex. A second mechanism for how the CIA targeting complex may influence FBXL5 function is as an allosteric activator of SCF^{FBXL5} that stimulates its IRP2 ubiquitin ligase activity in a manner distinct from IRP binding. Finally, the CIA targeting complex could be responsible for localizing SCF^{FBXL5} to a subcellular region in which IRPs are accessible as substrates. Future work will establish the mechanism and potentially combination of mechanisms by which the regulation of FBXL5 by the CIA targeting complex promotes its capacity for IRP degradation.

MAGE-F1-NSE1 E3 ubiquitin ligase complex has been recently shown to interact with and mediate ubiquitination and degradation of MMS19 and thus regulate the function of CIA targeting complex (Weon et al, 2018). Despite MAGE-F1 and FBXL5 both being E3 ligases associated with MMS19, there is little evidence at the moment to suggest that these pathways functionally overlap. Nonetheless, future studies examining how the activity and/or function of these E3 ligases might be coordinated in the context of iron and oxygen metabolism or contribute to the pathology of MAGE-F1-associated cancers is an important future question to address.

FBXL5 is not only a sensor of bioavailable iron but also molecular oxygen. Previous studies have argued for distinct mechanisms of iron and oxygen sensing by FBXL5 based upon conformational changes that ensue upon changes in iron or oxygen levels (Chollangi et al., 2012). In this study, we show that under low oxygen conditions there is dissociation of the complex between FBXL5 and the CIA targeting machinery. Although the exact mechanism remains unknown, we speculate that it could result from unknown factors that compete with the CIA targeting complex for binding to the CTBD domain of FBXL5 under low oxygen conditions. Another plausible explanation could be a hypoxia-specific post-translational modification of the CTBD domain that precludes binding of CIA targeting complex. It is intriguing to note that the stability of FBXL5 is diminished in hypoxia (Fig. 5A–D) and enhanced by overexpression of components of CIA targeting complex (Fig. 2A). Thus, the impaired interaction between FBXL5 and the CIA targeting complex in hypoxia may contribute to the reduced stability of FBXL5 in low oxygen conditions and highlights the existence of an oxygen-controlled regulatory mechanism that modulates FBXL5 stability independently of FBXL5's hemerythrin domain.

The effect of hypoxia on IRP2 has been well-documented (Vashisht et al., 2009; Hanson et al., 2003; Meyeron-Holtz et al., 2004). Hypoxia stimulates FBXL5 degradation and a corresponding increase in IRP2 levels. We show here that hypoxia also impairs the interaction between the CIA targeting complex and FBXL5 similarly leading to IRP2 accumulation (Fig. 5A and S8). This suggests that cells employ multiple redundant

mechanisms to turn off FBXL5-dependent IRP2 degradation and ensure that IRP2 accumulates in low O_2 conditions. The presence of multiple signaling axes for modulating the FBXL5-IRP2 relationship also provides opportunities for uncoupling iron sensing from oxygen sensing or iron availability from the integrity of the Fe-S cluster assembly pathway. This ability to fine-tune IRP-regulated iron and oxygen homeostasis is likely a key feature underlying these complex signaling networks that impinge upon FBXL5 function.

Star Methods

Further information and requests for resources and reagents should be directed to and will be fulfilled by the Lead Contact, James A. Wohlschlegel (jwohl@ucla.edu).

Experimental Model and Subject Details

HEK293 (ATCC, sex: female), Flp-In™ T-REx™ 293 cells (ThermoFisher Scientific, sex: female) and HEK293T cells (ATCC, sex: female) were utilized for the study. All cell lines were maintained at 37°C, 5% CO_2 in DMEM containing 4.5g glucose/L (Gibco by Life Technologies) supplemented with 10% fetal bovine serum (Gemini Bioproducts), 1X antibiotic-antimycotic (Gibco by Life Technologies) and 2mM L-glutamine (Gibco by Life Technologies). For hypoxia studies, cells were maintained in a gaseous mixture of 1% O_2, 5% CO_2 and 94% N_2 at 37°C for 16 hours. To induce gene expression in Flp-In™ T-REx™ 293 cells, doxycycline (Fisher Scientific) was added to the culture media at a final concentration of 1mg/mL every 24 hours before harvesting cells for analysis as indicated.

Method Details

Plasmids—The generation of pcDNA5-FRT/TO-3xHA-3xFLAG-FBXL5-WT, pcDNA5-FRT/TO-3xHA-3xFLAG-FBXL5-ΔFbox, pcDNA5-FRT/TO-3xHA-3xFLAG-FBXL5-C500, pcDNA3–6xMyc-FBXL5-WT, pcDNA3–6xMyc-FBXL5-C500, pcDNA3–6xMyc-FBXL5-ΔFbox and pcDNA5-FRT/TO-3xHA-3xFLAG-MMS19 has been described earlier *(*Vashisht et al., 2009; Stehling et al., 2012*)*. FBXL5-ΔCTBD and FBXL5-C500-ΔCTBD were generated using overlap-extension PCR with pCR8-FBXL5 and pDONR221-FBXL5-C500, respectively (described previously in Vashisht et al., 2009) serving as templates and primers designed to delete region spanning 1246–1752 bp region (corresponding to 470–592 amino acids) of wild-type gene and flanked by AttB1 and AttB2 sequences. FBXL5-ΔCTBD and FBXL5-C500-ΔCTBD fragments thus obtained were cloned into pDONR221 followed by subcloning into DEST plasmids pcDNA3–6xMyc and pcDNA5-FRT/TO-3xHA-3xFLAG using Gateway cloning system (Invitrogen) to generate pcDNA5-FRT/TO-3xFLAG-FBXL5-ΔCTBD, pcDNA5-FRT-TO-3xFLAG-FBXL5-C500-ΔCTBD, pcDNA3–6xMyc-FBXL5-ΔCTBD, and pcDNA3–6xMyc-FBXL5-C500-ΔCTBD. Human FAM96B and CIAO1 ORFs, purchased from Open Biosystems, served as the template for amplification of FAM96B and CIAO1 using primers flanked with AttB1 and AttB2 sequences. FAM96B and CIAO1 fragments were subsequently cloned in pDONR221 using Gateway cloning system (Invitrogen). To generate CFP-MMS19 and CFP-FAM96B, pDONR221 containing MMS19 (as described in Stehling et al., 2012) and FAM96B ORFs were subcloned into pDEST-pcDNA3-CFP using Gateway cloning system (Invitrogen). To generate pEBG-FAM96B and pCDNA-5-FRT/TO-3xHA-3xFLAG-FAM96B, pDONR221 containing FAM96B ORF was

subcloned into DEST plasmids pDEST-EBG and pcDNA5-FRT/TO-3xHA-3xFLAG using Gateway cloning system (Invitrogen). To generate pEBG-CIAO1, pDONR221 containing CIAO1 ORF was subcloned into DEST plasmids pDEST-EBG using Gateway cloning system (Invitrogen). FBXL5-CTBD-WT (470–592 amino acids of wild-type FBXL5), FBXL5-CTBD-CA (all cysteines mutated to alanines) and FBXL5-CTBD-CS (all cysteines mutated to Serines) were chemically synthesized (Integrated DNA Technologies). The fragments were then amplified using gene-specific primers flanked with AttB1 and AttB2 sequences. FBXL5-CTBD-WT, FBXL5-CTBD-CA and FBXL5-CTBD-CS fragments were then cloned into pDONR221 followed by recombination into the DEST plasmid pcDNA3–6xMyc using Gateway cloning system (Invitrogen) to generate pcDNA3–6xMyc-FBXL5-CTBD-WT, pcDNA3–6xMyc-FBXL5-CTBD-CA and pcDNA3–6xMyc-FBXL5-CTBD-CS. FAM96B deletion mutant sequences corresponding to 1–103 and 1–110 amino acids were generated by amplification using FAM96B wild-type as template and gene-specific primers flanked by AttB1 and AttB2 sequences. FAM96B mutant sequences corresponding to 1–110 amino acids with alanine substitutions at residues 104–110 were chemically synthesized (Integrated DNA Technologies) and amplified using gene-specific primers flanked by AttB1 and AttB2 sequences. The resulting PCR products were cloned into pDONR221 followed by recombination into the DEST plasmid pcDNA3–6xMyc using Gateway cloning system (Invitrogen) to generate pcDNA3–6xMyc-FAM96B-1–103aa, pcDNA3–6xMyc-1–110aa and pcDNA3–6xMyc-FAM96B-104–110-all-Ala. 2xFLAG-IRP1, 2xFLAG-IRP1-C3S, 2xFLAG-IRP2, HA-Ub, Myc-CUL1 and Myc-SKP1 were previously described (Johnson and Blobel, 1997; Zumbrennen et al., 2009). Plasmids utilized for generating dCas9/CRISPRi cell lines have been described in the section entitled ‘lentiviral preparation, lentiviral infection and generation of dCas9/CRISPRi cell lines’.

Generation of stable cell lines—Generation of Flp-In™ T-REx™ 293 cells stably expressing 3xHA-3xFLAG-FBXL5, 3xHA-3xFLAG-FBXL5-ΔFbox, 3xHA-3xFLAG-FBXL5-C500 and 3xHA-3xFLAG-MMS19 has been described previously (Vashisht et al., 2009; Stehling et al., 2012). Generation of doxycycline-inducible stable cell lines for knockdown of MMS19 (shMMS19) and FAM96B (shFAM96B) has been described earlier (Stehling et al., 2012). Flp-In™ T-REx™ 293 cells stably expressing 3xHA-3xFLAG-FBXL5-ΔCTBD, 3xHA-3xFLAG-FBXL5-C500-ΔCTBD, 3xHA-3xFLAGFAM96B and 3xHA-3xFLAG-FAM96A were generated using the Flp-In system (Invitrogen) according to the manufacturer’s protocol.

Lentiviral preparation, lentiviral infection and generation of dCas9/CRISPRi cell lines

1. The lentiviral plasmid pLV hU6-sgRNA hUbC-dCas9-KRAB-T2a-Puro encoding dCas9-KRAB was a gift from Charles Gersbach (Addgene plasmid #71236) (Thakore et al., 2015). The gRNA against FBXL5 was synthesized (IDT-DNA), hybridized, phosphorylated, and inserted into this plasmid using BsmBI sites.
2. To produce VSV-G pseudotyped lentivirus, HEK293T cells were co-transfected with the pLV hU6-sgRNA-FBXL5-hUbC-dCas9-KRAB-T2a-Puro lentiviral

expression plasmid, the second-generation packaging plasmid psPAX2 (Gift from Didier Trono, Addgene #12260) and envelope plasmid pMD2.G (Gift from Didier Trono, Addgene #12259). Conditioned medium containing lentivirus was collected 24 and 48 hours post-transfection.

3. Flp-In™ T-REx™ 293 cells were transduced with lentivirus to stably express dCas9-KRAB and U6-sgRNA-FBXL5. Puromycin was used to initiate selection of transduced cells (*FBXL5*-KD) approximately 96 hours after transduction.

4. Step3 was repeated for Flp-In™ T-REx™ 293 cells stably expressing 3xHA-3xFLAG-FBXL5-WT and 3xHA-3xFLAG-FBXL5-ΔCTBD, to generate *FBXL5*-KD$^{FBXL5\text{-}WT}$ and *FBXL5*-KD$^{FBXL5\text{-}\Delta CTBD}$ respectively.

Affinity purification of FBXL5-WT-containing protein complexes—Six 15 cm tissue culture plates each of Flp-In 293 or Flp-In 293 stably expressing 3XHA-3-Flag-tagged FBXL5 were grown, harvested and lysed in IP buffer constituted of 100mM Tris-HCl pH8.0, 150mM NaCl, 50mM EDTA, 0.1% NP-40, 10% glycerol, 1mM DTT, protease inhibitors and phosphatase inhibitors. Each of the normalized clarified protein lysates was incubated with 100uL of EZ-view anti-HA agarose (Pierce) for 2 hours at 4°C. Beads were washed four times using 1 mL of IP buffer per wash followed by washes with IP buffer lacking NP-40. Following the washes, bound protein complexes were eluted using 8M urea and 100mM Tris-Cl pH 8.0. The eluates were precipitated in acetone.

Proteomic characterization of affinity purified FBXL5 samples—Acetone precipitates were resuspended in 100mM Tris-HCl pH 8.5, 8M urea, reduced and alkylated using 5mM Tris (2-carboxyethyl) phosphine and 10mM iodoacetamide, respectfully, and proteolytically digested with Lys-C and trypsin. The digested peptides were subjected to offline high pH reverse phase fractionation using Pierce high pH reversed phase spin columns and subsequently analyzed by LC-MS/MS. Briefly, peptides were separated by reversed phase chromatography using 75 μm inner diameter fritted fused silica capillary column packed in-house to a length of 25 cm with Luna C18 3μm reverse phase particles. The increasing gradient of acetonitrile was delivered by a Dionex Ultimate 3000 (Thermo Scientific) at a flow rate of 300nL/min. MS/MS spectra were collected using data dependent acquisition on Orbitrap Fusion Lumos Tribrid mass spectrometer. Proteomic database search was performed using the MSGF+ algorithm via the target-decoy strategy against the EMBL Human reference proteome (UP000005640 9606) (Granholm et al., 2014). Identification false detection rates (FDRs) at the peptide-spectrum-match and protein levels were estimated by Percolator and FIDO, respectively, and filtered to achieve a 1% FDR (Serang et al., 2010). SAINTexpress was used to identify proteins significantly enriched in FBXL5 IPs but not control IPs (Teo et al., 2014). The mass spectrometry data have been deposited to the ProteomeXchange Consortium (http://proteomecentral.proteomexchange.org) via the MassIVE repository with the identifier PXD013697.

Immunoprecipitation—Cell lysates were prepared using immunoprecipitation (IP) buffer constituted of 100mM Tris-HCl pH 8.0, 150mM NaCl, 50mM EDTA, 0.1% NP-40, 10% glycerol, 1mM DTT, protease inhibitors and phosphatase inhibitors. Equal protein amounts

were incubated for 2 hours at 4°C with appropriate affinity matrix pre-equilibrated using IP buffer. Beads were washed 4 times in IP buffer followed by eluting bound protein complexes in 2X SDS dye. For immunoblotting, immunoprecipitates and whole cell lysates were boiled in SDS loading buffer, resolved on SDS-PAGE, followed by transfer onto PVDF membrane. The membranes were blocked in either 5% milk or BSA followed by incubation with appropriate primary antibody and HRP-labeled secondary antibody. Protein bands on membranes were visualized using Pierce ECL western blotting substrate (ThermoFisher).

Biotin pull-down assay—The protocol was adapted from Cho et al., 2010. Biotinylated RNA oligonucleotides, H-ferritin IRE-WT and H-ferritin IRE-Mut, were purchased from IDT. Cells were lysed in ribonucleoprotein immunoprecipitation buffer (containing 25mM Tris-HCl pH 7.5, 1% NP-40, 0.5% sodium deoxycholate, 150mM NaCl, protease inhibitor, phosphatase inhibitor, 1mM DTT and RNase inhibitor). 100 μg of each lysate was incubated with 100nM WT and Mut IRE for 3 h at room temperature to allow formation of IRP-biotinylated-IRE complexes. For purification of these complexes, the lysates were further incubated for 1 hour at room temperature with Pierce™ High Capacity Streptavidin Agarose (ThermoFisher) which had been pre-equilibrated with ribonucleoprotein immunoprecipitation buffer. After elution using 2X SDS dye, the IRP-Biotinylated-IRE complexes were resolved on SDS-PAGE and immunoblotted using IRP1 and IRP2. Protein bands on membranes were visualized using Pierce ECL western blotting substrate (ThermoFisher).

Ubiquitination assay—HEK293 cells were transfected with plasmids expressing HA-Ubiquitin, 2xFLAG IRP construct (2xFLAG-IRP2, 2x-FLAG-IRP1, or 2x-FLAG-IRP1-C3S) and either 6xMyc-FBXL5, 6xMyc-FBXL5-ΔCTBD, or vector control. Twenty-four hours post-transfection cells were treated with 10 μM MG132 for 2 hours. Cells were harvested and lysed under denaturing conditions as described previously (Bloom and Pagano, 2005). Ubiquitin conjugates were purified using anti-HA beads and the presence of IRP1 or IRP2 in the purified ubiquitin conjugates was detected by immunoblotting with FLAG M2 antibody.

Cell transfections and treatments—HEK293 cells were transiently transfected with indicated plasmids using either BioT (Bioland, Long Beach, CA), Lipofectamine™2000 or Lipofectamine™3000 following manufacturers' protocol. Cells were treated with following drugs/inhibitors at concentration and for time periods as indicated: FAC (100μg/mL) for 8 hours; DFO (100μM) for 8 hours, MG132 (10μM) for 2 hours; DMOG (0.5mM) for 24 hours and $CoCl_2$ (100μM) for 16 hours. siRNA transfections were carried out using Lipofectamine®RNAiMax as the transfection reagent and siGENOME SMARTpool FBXL5 siRNA (Dharmacon #M-012424–01-0005), siGENOME SMARTpool MMS19 siRNA (Dharmacon #M-017823–01), siGENOME SMARTpool FAM96B siRNA (Dharmacon #M-020340–02), siGENOME SMARTpool CIAO1 siRNA (Dharmacon #M-019857–02) and siGENOME Non-targeting siRNA (Dharmacon #D-001210–03-20). Manufacturer's instructions were followed for the transfections.

For hypoxia treatment, cells growing at 60% confluence were transferred to a hypoxia chamber (STEMCELL technologies) which was purged with a gaseous mixture of 1% O_2,

5% CO_2 and 94% N_2 for 7 minutes at a rate of 20 L/min using Single Flow Meter (STEMCELL Technologies, Cat. #27311). The sealed chamber was then transferred to 37°C and cells incubated for 16 hours before harvesting for further analysis.

To induce gene expression in Flp-In™ T-REx™ 293 stable cell lines, doxycycline was maintained in culture medium at a final concentration of 1μg/mL for 24–48 hours before harvesting cells for analysis. To accomplish efficient knockdown of target genes in lentiviral doxycycline-inducible shRNA knockdown cell lines, doxycycline was maintained in the culture medium at a final concentration of 1μg/mL for 9 days before cells were harvested for further analysis. Doxycycline was replenished every 24 hours.

Quantitative Real-time Reverse Transcript (qRT)-PCR—Total RNA was prepared using the Aurum Total RNA Mini-kit (Biorad). qRT-PCR was performed using iTaq Universal SYBR Green One-Step Kit (Biorad) for RT-qPCR on Stratagene Mx3000P using primer sets for human TfR1 (5'-TTGCGGCGAAGTCCAGTGTG-3', 5'-CCTGCAGTCCAGCTGGCAAA-3'), DMT1 (5'-TCTGGGCAGTGGGGATCCTG-3', 5'-GACGAGCAGGGTGGGGATGA-3') and actin (5'-ACCAACTGGGACGACATGGAGAAA3', 5' -TAGCACAGCCTGGATAGCAACGTA-3') as a control. The thermal cycle conditions were as follows: 10 min at 50°C and 10 min at 95°C followed by 40 cycles of 95°C for 30 sec, 60°C for 30 sec and 72°C for 30 sec. Dissociation curve was performed at 95°C for 1 min and 55–95°C ramp at the instrument default rate of 0.2°C/sec, with fluorescence data collection continuously on the 55–95°C ramp. All tests were performed in triplicate and all experiments were repeated three times. The mathematical transformations for primary data analysis were done by MxPro (Agilent). The amplification data were analyzed based on $2^{-\Delta\Delta CT}$ method. The results shown as histograms were expressed as fold changes of the treatment groups compared to the controls. p-values were determined by using Student's t-test.

In-vitro binding assay using GST-IRP2 and purified FLAG-tagged FBXL5 and ΔCTBD—Flp-In-293 cells stably expressing 3XHA-3XFlag-tagged FBXL5 and 3XHA-3-Flag-tagged FBXL5- ΔCTBD were induced with doxycycline for 16 hours. FLAG-tagged proteins were immunoprecipitated using anti-FLAG-M2 agarose beads and eluted using FLAG peptide. GST-tagged IRP2 transiently overexpressed in HEK293 cells was immunoprecipitated using Glutathione agarose and washed with high salt buffer to remove bound proteins. In-vitro binding assays were set up with equal amounts of either purified FLAG-tagged FBXL5 or FBXL5- ΔCTBD along with GSH-agarose bound GST-IRP2.

Supplementary Material

Refer to Web version on PubMed Central for supplementary material.

Acknowledgements

We thank Charles Gersbach for providing us with the lentiviral plasmid pLV hU6-sgRNA hUbC-dCas9-KRAB-T2a-Puro encoding dCas9-KRAB and Didier Trono for providing psPAX2 and pMD2.G. This work was supported by the National Institutes of Health GM089778 and GM112763 to JAW. W.D.B. was supported by the Ruth L. Kirschstein National Research Service Award GM007185 from the National Institutes of Health.

References

Bloom J, and Pagano M (2005) Experimental tests to definitively determine ubiquitylation of a substrate. Methods Enzymol 399, 249–66. [PubMed: 16338361]

Cho HH, Cahill CM, Vanderburg CR, Scherzer CR, Wang B, Huang X, and Rogers JT (2010) Selective translational control of the Alzheimer amyloid precursor protein transcript by iron regulatory protein-1. J Biol Chem 285, 31217–32. [PubMed: 20558735]

Chollangi S, Thompson JW, Ruiz JC, Gardner KH, and Bruick RK (2012) Hemerythrin-like domain within F-box and leucine-rich repeat protein 5 (FBXL5) communicates cellular iron and oxygen availability by distinct mechanisms. J Biol Chem 287, 23710–7. [PubMed: 22648410]

Fuss JO, Tsai CL, Ishida JP, and Tainer JA (2015) Emerging critical roles of Fe-S clusters in DNA replication and repair. Biochim Biophys Acta 1853, 1253–71. [PubMed: 25655665]

Gari K, León Ortiz AM, Borel V, Flynn H, Skehel JM, and Boulton SJ (2012) MMS19 links cytoplasmic iron-sulfur cluster assembly to DNA metabolism. Science 337, 243–245. [PubMed: 22678361]

Granholm V, Kim S, Navarro JC, Sjölund E, Smith RD, Käll L (2014). Fast and accurate database searches with MS-GF+Percolator. J Proteome Res 13, 890–897. [PubMed: 24344789]

Hanson ES, Rawlins ML, and Leibold EA (2003) Oxygen and iron regulation of iron regulatory protein 2. J Biol Chem 278, 40337–40342. [PubMed: 12888568]

Johnson ES, and Blobel G (1997) Ubc9p is the conjugating enzyme for the ubiquitin-like protein Smt3p. J Biol Chem 272, 26799–802. [PubMed: 9341106]

Johnson NB, Deck KM, Nizzi CP, and Eisenstein RS (2017) A synergistic role of IRP1 and FBXL5 proteins in coordinating iron metabolism during cell proliferation. J Biol Chem 292, 15976–15989. [PubMed: 28768766]

Kim KS, Maio N, Singh A, and Rouault TA (2018) Cytosolic HSC20 integrates de novo iron-sulfur cluster biogenesis with the CIAO1-mediated transfer to recipients. Hum Mol Genet 27, 837–852. [PubMed: 29309586]

Maione V, Cantini F, Severi M, and Banci L (2018) Investigating the role of the human CIA2A-CIAO1 complex in the maturation of aconitase. Biochim Biophys Acta

Majmundar AJ, Wong WJ, and Simon MC (2010) Hypoxia-inducible factors and the response to hypoxic stress. Mol Cell 40, 294–309. [PubMed: 20965423]

Meyron-Holtz EG, Ghosh MC, and Rouault TA (2004). Mammalian tissue oxygen levels modulate iron-regulatory protein activities in vivo. Science 306, 2087–2090. [PubMed: 15604406]

Muckenthaler MU, Rivella S, Hentze MW, and Galy B (2017) A Red Carpet for Iron Metabolism. Cell 168, 344–361. [PubMed: 28129536]

Odermatt DC, and Gari K (2017). The CIA Targeting Complex Is Highly Regulated and Provides Two Distinct Binding Sites for Client Iron-Sulfur Proteins. Cell Rep 18, 1434–1443. [PubMed: 28178521]

Outten CE, and Albetel AN (2013) Iron sensing and regulation in Saccharomyces cerevisiae: Ironing out the mechanistic details. Curr Opin Microbiol 16, 662–8. [PubMed: 23962819]

Rouault TA and Maio N (2017). Biogenesis and functions of mammalian iron-sulfur proteins in the regulation of iron homeostasis and pivotal metabolic pathways. J Biol Chem 292, 12744–12753. [PubMed: 28615439]

Ruiz JC, and Bruick RK (2014). F-box and leucine-rich repeat protein 5 (FBXL5): sensing intracellular iron and oxygen. J Inorg Biochem 133, 73–77. [PubMed: 24508277]

Salahudeen AA, Thompson JW, Ruiz JC, Ma HW, Kinch LN, Li Q, Grishin NV, and Bruick RK (2009). An E3 ligase possessing an iron-responsive hemerythrin domain is a regulator of iron homeostasis. Science 326, 722–726. [PubMed: 19762597]

Serang O, MacCoss MJ, Noble WS (2010). Efficient marginalization to compute protein posterior probabilities from shotgun mass spectrometry data. J Proteome Res 9, 5346–5357. [PubMed: 20712337]

Sharma AK, Pallesen LJ, Spang RJ, and Walden WE (2010). Cytosolic iron-sulfur cluster assembly (CIA) system: factors, mechanism, and relevance to cellular iron regulation. J Biol Chem 285, 26745–51. [PubMed: 20522543]

Stehling O, Mascarenhas J, Vashisht AA, Sheftel AD, Niggemeyer B, Rösser R, Pierik AJ, Wohlschlegel JA, and Lill R (2013). Human CIA2A-FAM96A and CIA2B-FAM96B integrate iron homeostasis and maturation of different subsets of cytosolic-nuclear iron-sulfur proteins. Cell Metab 18, 187–198. [PubMed: 23891004]

Stehling O, Vashisht AA, Mascarenhas J, Jonsson ZO, Sharma T, Netz DJ, Pierik AJ, Wohlschlegel JA, and Lill R (2012). MMS19 assembles iron-sulfur proteins required for DNA metabolism and genomic integrity. Science 337, 195–199. [PubMed: 22678362]

Teo G, Liu G, Zhang J, Nesvizhskii AI, Gingras AC, Choi H (2014). SAINTexpress: improvements and additional features in Significance Analysis of INTeractome software. J Proteomics 100, 37–43. [PubMed: 24513533]

Thakore PI, D'Ippolito AM, Song L, Safi A, Shivakumar NK, Kabadi AM, Reddy TE, Crawford GE, and Gersbach CA (2015). Highly specific epigenome editing by CRISPR-Cas9 repressors for silencing of distal regulatory elements. Nat Methods 12, 1143–9. [PubMed: 26501517]

Torti SV, and Torti FM (2013). Iron and cancer: more ore to be mined. Nat Rev Cancer 13, 342–55. [PubMed: 23594855]

Vashisht AA, Zumbrennen KB, Huang X, Powers DN, Durazo A, Sun D, Bhaskaran N, Persson A, Uhlen M, Sangfelt O, et al. (2009). Control of iron homeostasis by an ironregulated ubiquitin ligase. Science 326, 718–721. [PubMed: 19762596]

Wu D, and Yotnda P (2011) Induction and testing of hypoxia in cell culture. J Vis Exp 54 pii: 2899.

Zumbrennen KB, Wallander ML, Romney SJ, and Leibold EA (2009) Cysteine oxidation regulates the RNA-binding activity of iron regulatory protein 2. Mol Cell Biol 29, 2219–29. [PubMed: 19223469]

Highlights

- CIA targeting complex interacts with but is not substrate of FBXL5
- CTBD domain of FBXL5 is critical for interaction with the CIA targeting complex
- CIA targeting complex stimulates FBXL5-mediated poly-ubiquitination of IRPs
- O_2 levels regulate the FBXL5-CIA targeting complex interaction

(A)

Protein	Uniprot	Spectral counts	Fold change	BFDR
FBXL5	Q9UKA1	323	3235	0
MMS19	Q96T76	84	7.04	0
CIAO1	O76071	53	2.86	0.02
FAM96B	Q9Y3D0	30	2.9	0.01

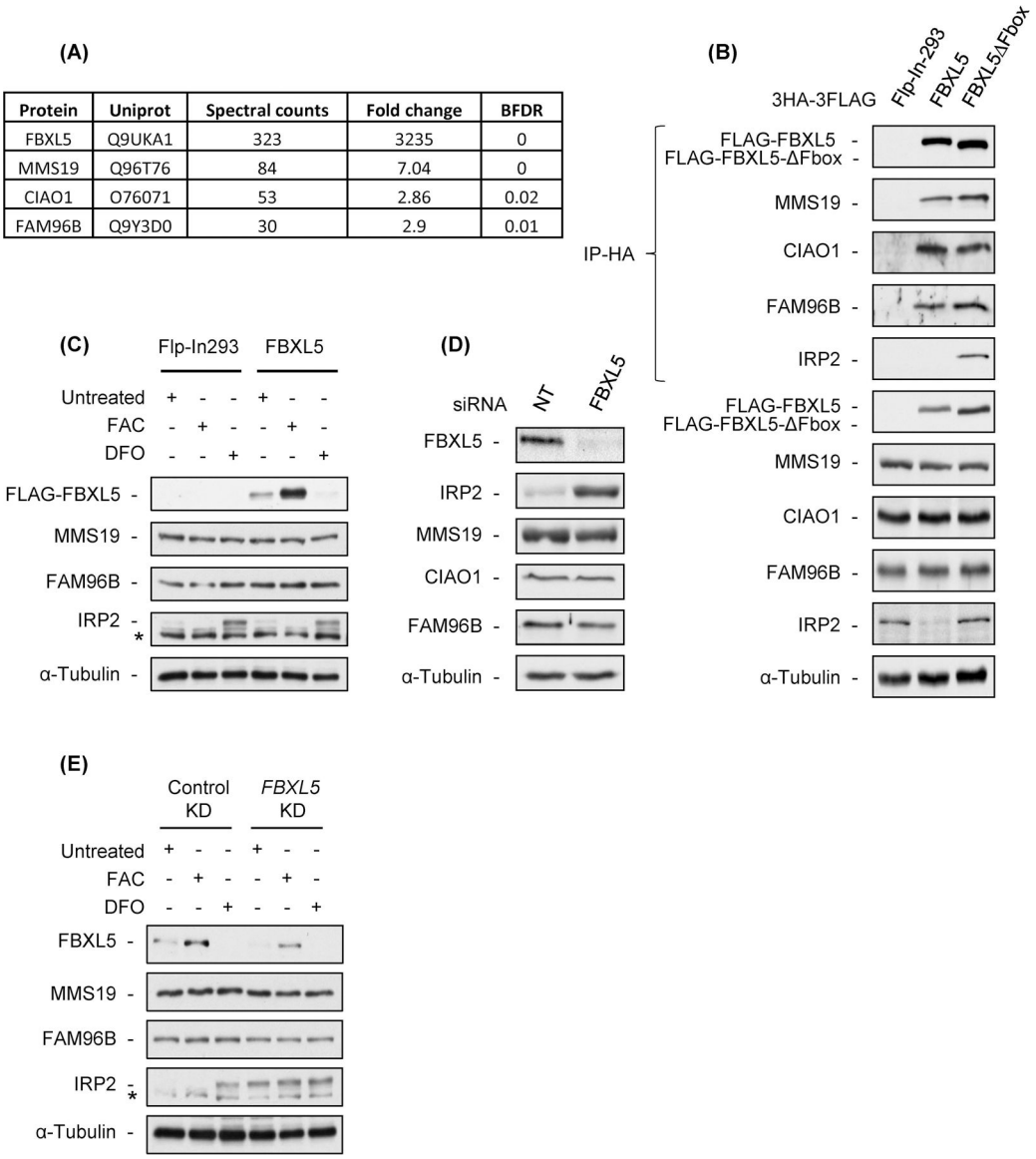

Figure 1. FBXL5, an E3 ubiquitin ligase substrate adaptor, interacts with CIA targeting complex without affecting its stability.

(A) Proteins interacting with FBXL5 were identified by mass spectrometry after immunoprecipitation of HA-FLAG-FBXL5 from Flp-In-293 cells stably overexpressing 3XHA-3XFLAG-FBXL5. CIA targeting complex components were present specifically in FBXL5 IPs but not control IPs. Spectral counts for each CIA targeting complex member in the FBXL5 IP as well as fold-enrichment over the control IP and BFDR were calculated by the SAINT algorithm and are listed in the table. (B) Whole cells lysates from Flp-In 293 control cells or cells stably overexpressing HA-FLAG-FBXL5 or FBXL5-ΔFbox were immunoprecipitated with anti-HA antibodies. HA immunoprecipitates (IP-HA) and whole cell extracts (WCE) were resolved by SDS-PAGE and immunoblotted with antibodies against FLAG, MMS19, CIAO1, FAM96B, IRP2 and α-tubulin. (C) Flp-In 293 cells stably overexpressing HA-FLAG-FBXL5 or control cells (Flp-In 293) were treated with FAC (100μg/mL) or DFO (100μM) for 8 hours. WCEs were immunoblotted with FLAG,

MMS19, FAM96B, IRP2 and α-tubulin antibodies. (D) HEK293 cells were treated with either non-targeting (NT) siRNA or siRNA targeted against FBXL5 for 24 hours. WCEs were immunoblotted with antibodies against FBXL5, IRP2, MMS19, CIAO1, FAM96B and α-tubulin. (E) Flp-In 293 cells were infected with lentiviral vectors expressing dCas9 with non-target (control KD) or FBXL5 specific gRNA (*FBXL5* KD). Control KD and *FBXL5*-KD cells were subjected to FAC (100μg/mL) or DFO (100μM) treatment for 8 hours. WCEs were immunoblotted with FBXL5, MMS19, FAM96B, IRP2 and α-tubulin antibodies. * denotes non-specific band in IRP2 panels.

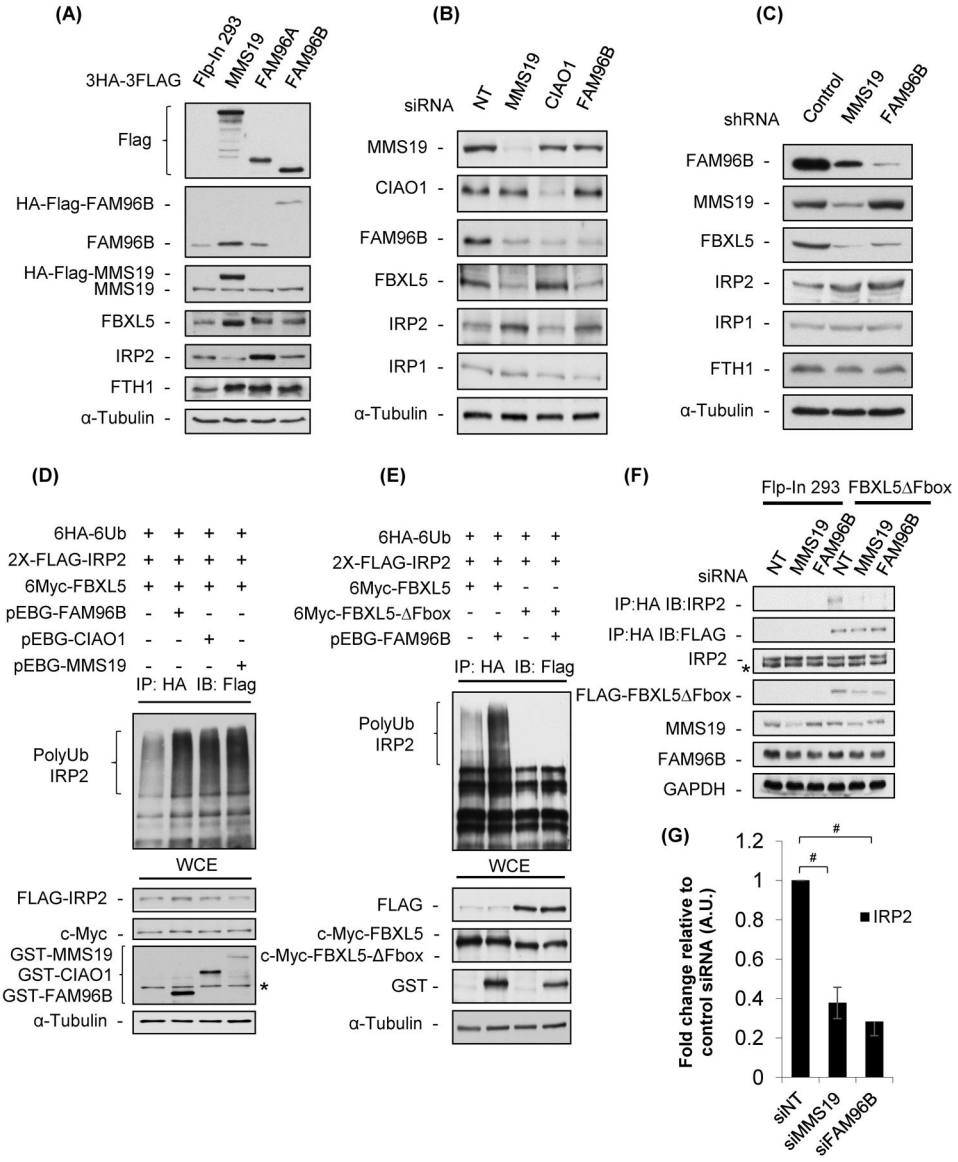

Figure 2. CIA targeting complex potentiates IRP2 poly-ubiquitination and degradation

(A) WCEs from control cells (Flp-In 293) or Flp-In 293 cells stably overexpressing HA-FLAG-tagged versions of MMS19, FAM96A or FAM96B were resolved by SDS-PAGE and immunoblotted with FLAG, FAM96B, MMS19, FBXL5, IRP2, FTH1 and α-tubulin antibodies. (B) HEK293 cells were treated with either non-targeting siRNA (NT) or siRNAs targeted against MMS19, CIAO1 or FAM96B. WCEs were immunoblotted with MMS19, CIAO1, FAM96B, FBXL5, IRP2, IRP1 and α-tubulin antibodies. (C) Flp-In 293 cells stably expressing shRNA against MMS19 or FAM96B and control cells were induced with doxycycline for 9 days to allow shRNA-mediated knockdown of the target genes. WCEs were immunoblotted using FAM96B, MMS19, FBXL5, IRP2, IRP1, FTH1 and α-tubulin antibodies. (D) HEK293 cells were co-transfected with HA-Ub and FLAG-IRP2 along with GST-tagged MMS19, FAM96B or CIAO1, treated with 15μM MG132 for 4 hours, and ubiquitin conjugates immunoprecipitated by using anti-HA antibodies. HA

immunoprecipitates (IP: HA) and WCEs were immunoblotted with FLAG, GST, Myc and α-tubulin antibodies. (E) HEK293 cells were co-transfected with HA-Ub, FLAG-IRP2, GST-FAM96B and either Myc-FBXL5 or Myc-FBXL5-ΔFbox and then treated with 15μM MG132 for 4 hours and ubiquitin conjugates immunoprecipitated by using anti-HA antibodies. HA immunoprecipitates (IP: HA) and WCEs were immunoblotted with antibodies against FLAG, Myc, GST and α-tubulin. (F) Control cells (Flp-In 293) or Flp-In 293 cells stably overexpressing HA-FLAG- FBXL5-ΔFbox were treated with either non-targeting siRNA (NT) or siRNAs targeted against MMS19 or FAM96B. Whole cell lysates were immunoprecipitated using beads conjugated to anti-HA antibodies. HA-immunoprecipitates and WCEs were immunoblotted using antibodies against IRP2, FAM96B, FLAG, MMS19 and GAPDH. (G) Quantitative representation of the experiment performed in F. Experiments are plotted as mean ± S.D. (n=3 independent experiments). The bars represent immunoprecipitated IRP2 normalized with immunoprecipitated HA-tagged FBXL5-ΔFbox. # denotes p value < 0.001. * denotes non-specific bands in GST and IRP2 panels.

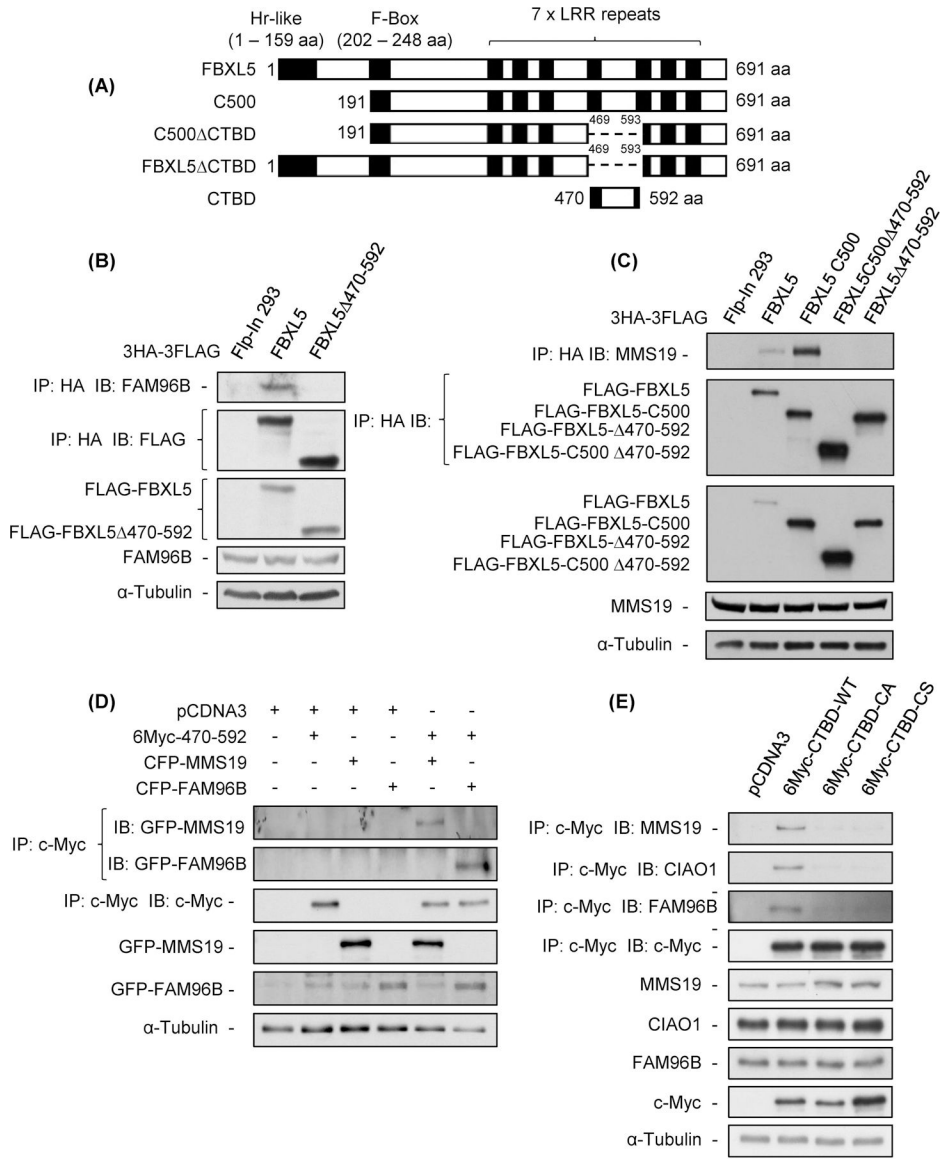

Figure 3. FBXL5 interacts with MMS19 and FAM96B via domain comprised of amino acids 470–592.

(A) Domain structure of FBXL5 and mutants. (B) Flp-In 293 cells stably overexpressing HA-FLAG tagged FBXL5-wildtype or FBXL5-ΔCTBD were induced with doxycycline for 24 hours. Whole cell lysates were immunoprecipitated using anti-HA antibodies. HA-immunoprecipitates and WCEs were immunoblotted using antibodies against FAM96B, FLAG and α-tubulin. (C) Flp-In 293 cells stably overexpressing HA-FLAG tagged versions of FBXL5, FBXL5-ΔCTBD, FBXL5-C500, and FBXL5-C500-ΔCTBD were induced with doxycycline for 24 hours. Whole cell lysates were immunoprecipitated using anti-HA antibodies. HA-immunoprecipitates and WCEs were immunoblotted using antibodies against MMS19, FLAG and α-tubulin. (D) HEK293 cells were transfected with pCDNA3 or Myc-FBXL5-CTBD together with either CFP-MMS19 or CFP-FAM96B. Binding partners of Myc-tagged proteins were immuno-purified using anti-myc antibodies. Myc-immunoprecipitates and WCEs were immunoblotted with antibodies against GFP, myc and

α-tubulin. (E) HEK293 cells were transfected with pCDNA3 or Myc-tagged versions of FBXL5-CTBD-WT, FBXL5-CTBD-CA (all cysteines substituted with alanines) or FBXL5-CTBD-CS (all cysteines substituted with serines). Binding partners of Myc-tagged proteins were immuno-purified using anti-myc antibodies. Myc-immunoprecipitates and WCEs were immunoblotted with antibodies against myc, MMS19, FAM96B and α-tubulin

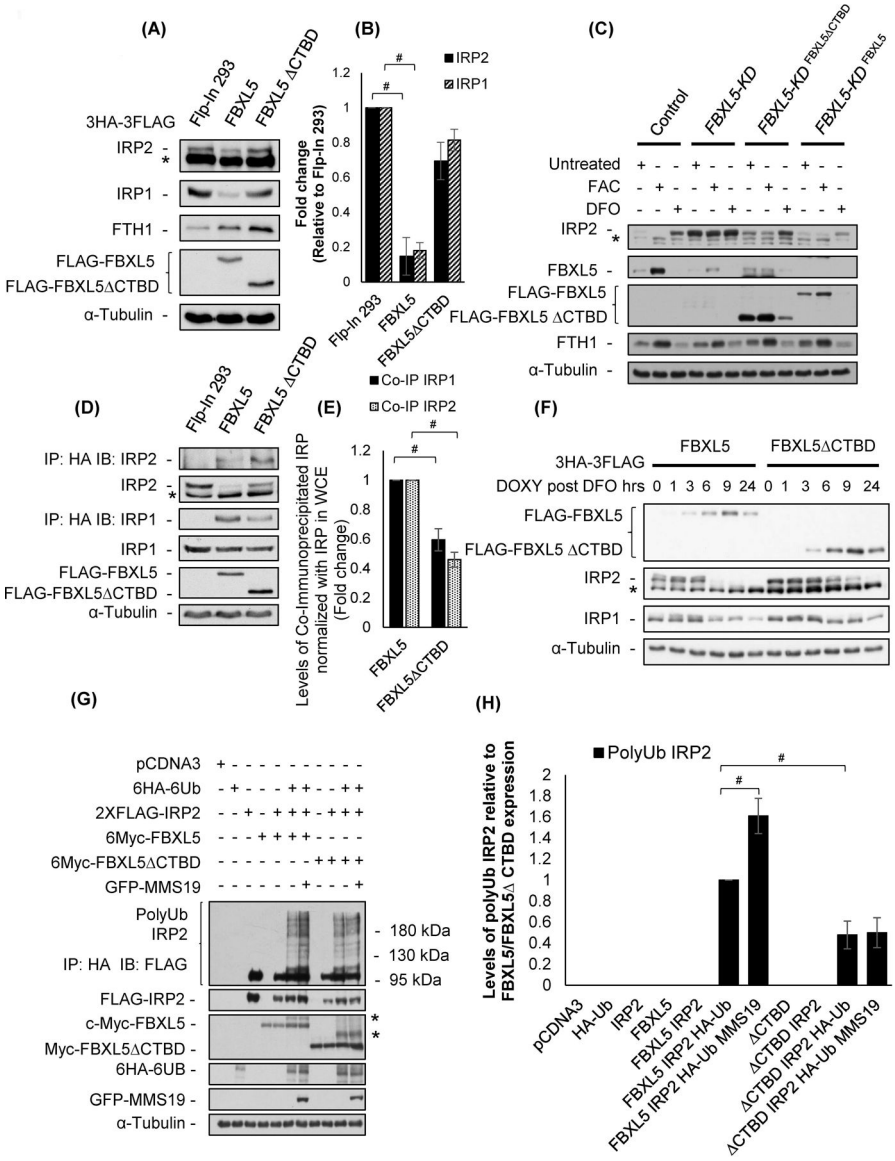

Figure 4. FBXL5-ΔCTBD is not as potent as wild-type FBXL5 in driving IRP2 Degradation

(A) Flp-In 293 cells stably overexpressing either HA-Flag-FBXL5 or FBXL5-ΔCTBD and control cells (Flp-In 293) were induced with doxycycline for 24 hours. WCEs were immunoblotted using antibodies for FLAG, IRP1, IRP2, FTH1 and α-tubulin. (B) Quantitative representation of the experiment performed in A. Experiments are plotted as mean ± S.D. (n=3 independent experiments). # denotes p value <0.001. (C) *FBXL5*-KD cells lines were further manipulated to stably express either HA-FLAG-FBXL5-WT (*FBXL5*-KD$^{FBXL5\text{-}WT}$) or HA-FLAG-FBXL5-ΔCTBD (*FBXL5*-KD$^{FBXL5\text{-}\Delta CTBD}$). These cell lines together with control KD cells were treated with FAC (100μg/mL) or DFO (100μM) for 8 h. WCEs were immunoblotted using antibodies against IRP2, FBXL5, FLAG, FTH1 and α-tubulin. (D) Whole cells lysates from FlpIn 293 control cells or cells stably overexpressing either HA-FLAG-FBXL5 or FBXL5-ΔCTBD were immunoprecipitated with anti-HA antibodies. HA immunoprecipitates (IP-HA) and WCE were resolved by SDS-

PAGE and immunoblotted with antibodies against FLAG, IRP2, IRP1 and α-tubulin. (E) Quantitative representation of the experiment performed in D. Experiments are plotted as mean ± S.D. (n=3 independent experiments). # denotes p value <0.001. The bars represent levels of co-immunoprecipitated IRP relative to the expression of IRP in WCE. (F) Flp-In 293 cells stably expressing either HA-FLAG-FBXL5 or FBXL5-ΔCTBD mutant were left uninduced and subjected to DFO treatment (100μM) for 16 hours. Following DFO treatment, cells were induced with doxycycline and harvested at indicated time points. WCEs were immunoblotted using antibodies against FLAG, IRP2, IRP1 and α-tubulin. (G) HEK293 cells were transfected with pCDNA3, 6HA-6Ub only, 2-FLAG-IRP2 only, 6-Myc-FBXL5 or 6- Myc-FBXL5-ΔCTBD alone or co-transfected with HA-Ub and FLAG-IRP2 along with Myc-FBXL5, Myc-FBXL5-ΔCTBD or pCDNA3 with or without GFP-MMS19 then treated with 10μM MG132 for 2 hours and ubiquitin conjugates immunoprecipitated using anti-HA antibodies. HA immunoprecipitates (IP: HA) and WCEs were immunoblotted with FLAG, myc and α-tubulin antibodies. (H) Quantitative representation of the experiment performed in F. Experiments are plotted as mean ± S.D. (n=3 independent experiments). The bars represent the levels of poly-ubiquitinated FLAG-IRP2 levels relative to the expression of either Myc-FBXL5 or MycFBXL5ΔCTBD. ## denotes p value < 0.005. * denotes non-specific bands in IRP2 and Myc panels.

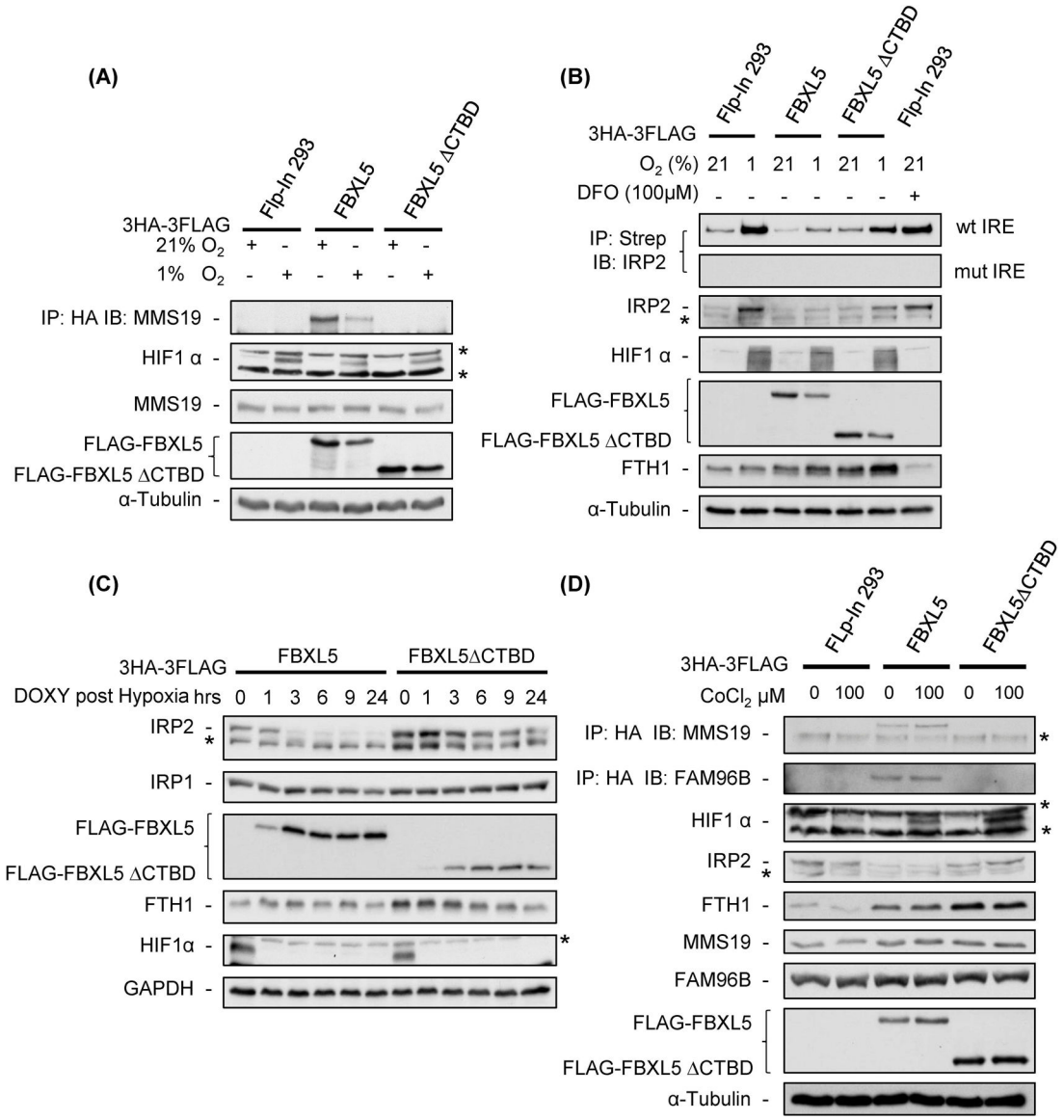

Figure 5. Interaction between FBXL5 and CIA targeting complex is oxygen-dependent.

(A) Flp-In 293 cells stably expressing HA-FLAG-tagged versions of FBXL5 or FBXL5-ΔCTBD and control cells (Flp-In-293) were subjected to either 21% or 1% O_2 for 16 hours. Whole cell lysates were immunoprecipitated using anti-HA antibodies. HA immunoprecipitates and WCEs were immunoblotted using antibodies specific for MMS19, HIF1α, FLAG and α-tubulin. (B) Flp-In 293 cells stably expressing HA-FLAG-FBXL5 or FBXL5-ΔCTBD and control cells (Flp-In-293) were subjected to either 21% or 1% O_2 for 16 hours. Flp-In 293 cells treated with 100μM DFO for 16 hours served as positive control. Whole cells lysates were incubated with biotin-labeled consensus (wt-IRE) or mutant IRE (mut-IRE) containing oligonucleotides followed by enrichment with streptavidin conjugated beads. Streptavidin-IRE bound proteins and WCEs were immunoblotted using antibodies against IRP1, IRP2, FTH1, HIF1α, FLAG and αtubulin. (C) Flp-In 293 cells stably expressing either HA-FLAG versions of FBXL5 or the FBXL5-ΔCTBD mutant were left

uninduced and subjected to 1% O_2 for 16 hours. Following hypoxia treatment, cells were shifted to normoxia simultaneous with doxycycline induction and harvested at indicated time points. WCEs were immunoblotted using antibodies against FLAG, IRP2, IRP1, FTH1, HIF1α and GAPDH. (D) Flp-In 293 cells stably expressing HA-FLAGFBXL5 or HA-FLAG-FBXL5-ΔCTBD and control cells (Flp-In-293) were subjected to either vehicle or $CoCl_2$ (100μM) for 16 hours. Whole cell lysates were immunoprecipitated using antiHA antibodies. HA immunoprecipitates and WCEs were immunoblotted using antibodies against MMS19, FAM96B, IRP2, IRP1, FTH1, HIF1α, FLAG and α-tubulin. * denotes non-specific bands in HIF1α□MMS19 and IRP2 panels.

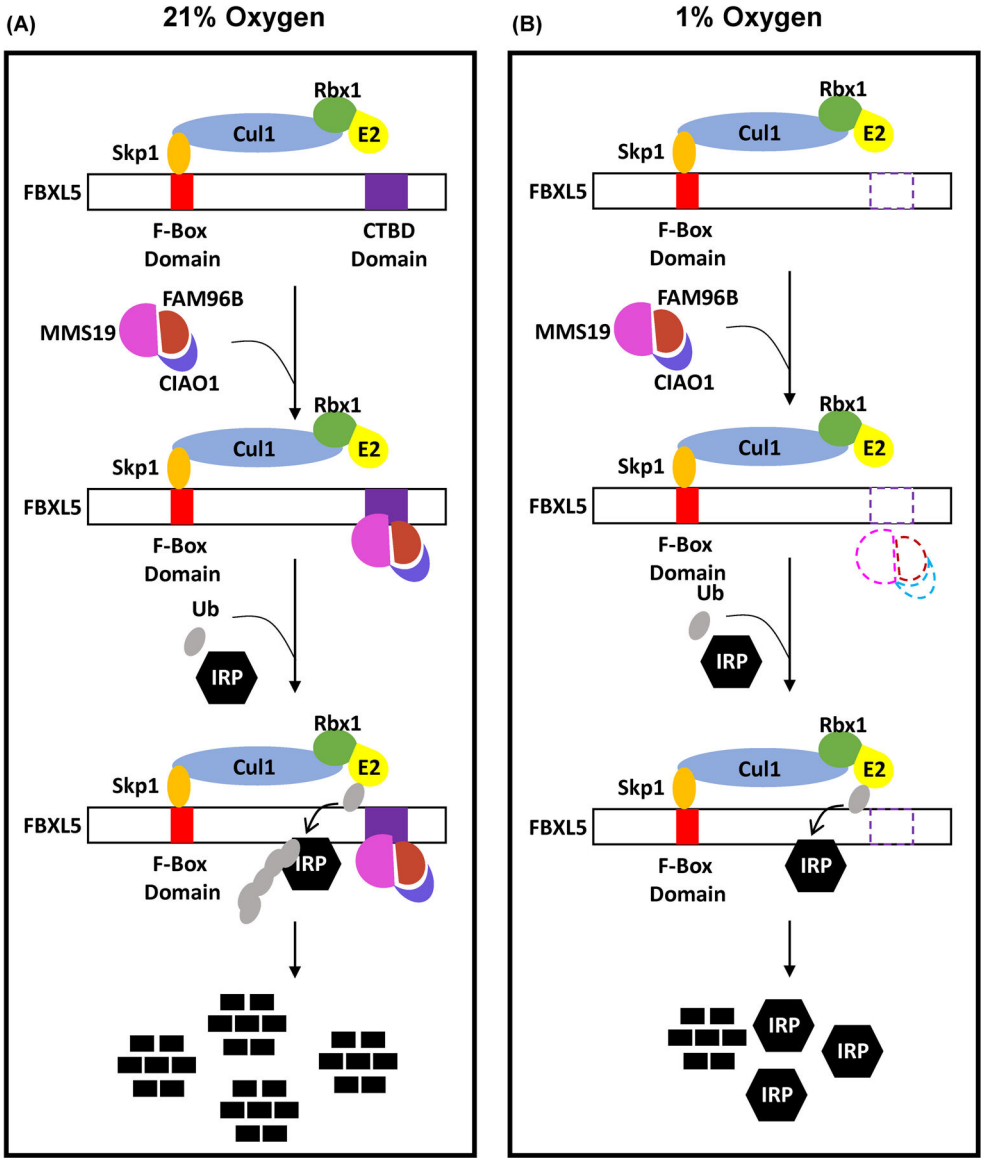

Figure 6. Interaction of FBXL5 with CIA targeting complex is O_2-sensitive and potentiates FBXL5-mediated degradation of IRPs.

(A) In 21% O_2, the interaction of FBXL5 with MMS19/FAM96B via the CTBD domain at its Cterminus promotes FBXL5-dependent ubiquitination and degradation of IRPs. (B) The loss of the interaction between the CIA targeting complex and FBXL5 in hypoxia impairs FBXL5dependent IRP degradation.